Fischer−Tropsch Synthesis on Anchored $Co/Nb_2O_5/Al_2O_3$ Catalysts: The Nature of the Surface and the Effect on Chain Growth

F. M. T. Mendes,[†] C. A. C. Perez,[†] F. B. Noronha,[‡] C. D. D. Souza,[†] D. V. Cesar,[†] H. J. Freund,[§] and M. Schmal*,[†]

Federal University of Rio de Janeiro−NUCAT-PEQ-COPPE, 128 Centro de Tecnologia Bl. G, Cidade Universitária, Rio de Janeiro, Brazil, Instituto Nacional de Tecnologia, Av. Venezuela 2, CEP 20081-310, Brazil, and Fritz-Haber Institut, Max Planck G., Faradayweg 4−6, Berlin, Germany

Received: January 10, 2006; In Final Form: March 10, 2006

A series of $Co/x\%Nb_2O_5/Al_2O_3$ catalysts were prepared by anchoring niobia on an Al_2O_3 support at different niobia concentrations. Characterization of the structure and nature of surface active sites was attempted in order to correlate the CO hydrogenation activity of these systems with those of the Co/Al_2O_3 and Co/Nb_2O_5 catalysts. The effect of the reduction temperature on the CO hydrogenation activity and selectivity was studied, showing that interaction of cobalt and niobia surface species favored the selectivity for hydrocarbon chain growth. However, this effect is less pronounced on the niobia-promoted Co/Al_2O_3 compared to Co/Nb_2O_5 catalysts. X-ray photoelectron spectroscopy (XPS) and diffuse reflectance spectroscopy (DRS) results on $Co/x\%Nb_2O_5/Al_2O_3$ showed prevailing amounts of Co^{2+} and Co^{3+} after calcination and reduction at 573 K, while, after reduction at 773 K, besides metallic cobalt, the Co^{2+} species still remains in contact with alumina, even for higher niobia loading. It seems that during this process formation and destruction of new interfaces involving Co^0-NbO_x sites takes place. Results suggest that Co^0, Co^0-Co^{2+}, and Co^0-NbO_x are the active sites at the surface. The relative abundance of Co^{2+} species affects greatly the performance of the catalysts. DRIFTS and selectivity results suggest that these sites might be responsible for the reaction chain growth and therefore for the drastic change in the selectivity of CH_4 and C_5^+ hydrocarbons mainly on the Co/Nb_2O_5 catalyst. DRIFTS results on $Co/Nb_2O_5/Al_2O_3$ showed the formation of $-C{=}C-$ and $-CH_3-$ besides CH_xO species. With increasing reduction temperature, the $-C{=}C-$ species disappear while $-CH_3-$ fragments increased markedly, suggesting the formation of increasing amounts of hydrocarbons with higher chain length.

1. Introduction

Natural gas is becoming more attractive as an energy source due to the increasing prices of oil, the huge reserves of gas, and environmental problems. This situation has driven many researchers to develop more economic processes of upgrading natural gas to higher hydrocarbon fuels. The Fischer−Tropsch (F−T) synthesis is an alternative route to produce liquid fuels from synthesis gas.

Cobalt based catalysts have been widely used in the $CO + H_2$ reaction for the production of hydrocarbons.[1−7] They were among several others to produce hydrocarbons from CO hydrogenation due to their ability to hydrogenate dissociated carbon species and promote chain growth. Cobalt is a typical metal that may adsorb CO molecules dissociatively forming carbon atoms at the surface, which may be hydrogenated, and it is an appropriate catalyst for the formation of long chain hydrocarbons.[8−12] However, the main problem of the F−T synthesis is the wide range of product distribution when conventional F−T catalysts are being used.[13] To overcome the selectivity limitations and to enhance the catalyst efficiency in CO hydrogenation, several approaches have been studied, such as the use of reducible supports[14,15] and the addition of a second metal component.[16−21]

In principle, the presence of a reducible oxide allows changes in the electronic or geometric structure, arrangement and size of particles, and adsorption properties.[16]

Niobium pentoxide as a support material for CO hydrogenation metal catalysts was the subject of a few studies.[5,14−15,22−27] These studies have reported that the use of Nb_2O_5 as a support results in higher CO hydrogenation activities for Rh/Nb_2O_5 in comparison to Rh supported on ZrO_2, Al_2O_3, SiO_2, or MgO[25] and for Ni/Nb_2O_5 in comparison to Ni/SiO_2.[26] Enhanced selectivity for high molecular weight hydrocarbons in CO hydrogenation over Co/Nb_2O_5[14,22] and Ni/Nb_2O_5,[27] compared to more traditional supports, such as Al_2O_3[14,22,27] and SiO_2,[22] was also observed.

In addition, niobia[4,14,15] and titania-supported[19,20] cobalt catalysts showed a high selectivity toward long chain hydrocarbons in the F−T synthesis after reduction at high temperature. These results might be explained by the formation of new sites during high temperature reduction.

In this study, we investigate the structure and surface properties of cobalt niobia/alumina systems, when niobia is coated at different concentrations over an alumina of high surface area ($Co/x\%Nb_2O_5/Al_2O_3$). The performance in a CO hydrogenation reaction, in an attempt to explain the effect of niobia on the product selectivity of Co-based catalysts, has been compared to the binary Co/Al_2O_3 and $Co/x\%Nb_2O_5$ systems. CO hydrogenation tests with in situ DRIFT data are discussed along with complementary characterizations by diffuse reflec-

* Corresponding author: schmal@peq.coppe.ufrj.br.
[†] Federal University of Rio de Janeiro−NUCAT-PEQ-COPPE.
[‡] Instituto Nacional de Tecnologia.
[§] Fritz-Haber Institut.

10.1021/jp060175g CCC: $33.50
Published on Web 04/19/2006

TABLE 1: Surface Areas (BET), Total Hydrogen Consumption during TPR, and Contents of Nb_2O_5 and Cobalt

sample	BET area ($m^2\ g^{-1}$)	Nb_2O_5 content (%)	Co content (%)	TPR total H_2 consumption (μmol g cat^{-1})[b]
Co/Al_2O_3	186.9		4.25	0.39
Co/Nb_2O_5	13.1	~95.50	4.50	1.58
$Co/5\%Nb_2O_5/Al_2O_3$	201.1	4.30	5.00[a]	0.46
$Co/20\%Nb_2O_5/Al_2O_3$	178.3	19.9	4.80	0.69

[a] Nominal. [b] The theoretical consumption of H_2 for $Co_3O_4 \Rightarrow Co^0$ is 1.17 μmol g cat^{-1}.

tance spectroscopy (DRS), and X-ray photoelectron spectroscopy (XPS) techniques.

2. Experimental Section

2.1. Catalyst Preparation. The niobium ammonium complex material obtained from CBMM (Companhia Brasileira de Metalurgia e Mineração (CBMM, AD 1264)) was calcined at a heating rate 2 K min^{-1} up to 873 K and kept at this temperature for 4 h to convert an amorphous phase to the crystalline form of niobium pentoxide. Alumina (Harshaw, BET area 197 $m^2\ g^{-1}$) was pretreated in an aerated furnace (50 mL min^{-1}) at 823 K for 16 h.

The $x\%Nb_2O_5/Al_2O_3$ ($x = 5$ and 20 weight of Nb_2O_5) was prepared by wet impregnation of alumina with a solution of an ammonium niobium complex in a rotator evaporator for 16 h, as described elsewhere.[4,5] After drying at 353 K, under vacuum, the sample was set in a furnace and heated at 373 K for 16 h, followed by calcination under flowing air at 823 K (2 K min^{-1}) for 16 h.

The cobalt catalyst was prepared by incipient wetness impregnation with a $Co(NO_3)_2 \cdot 6H_2O$ (Riedel-de Häen, 99% purity) solution. The Co content was kept constant at approximately 5 wt %.[1,5] After impregnation, all catalysts were dried overnight at 383 K followed by calcination at 2 K min^{-1} up to 673 K, kept at this temperature for 3 h, and stored for characterization and catalytic tests. Table 1 shows Nb_2O_5 and cobalt contents plus the total hydrogen consumption during temperature programmed reaction (TPR) experiments. Cobalt concentrations were determined by atomic absorption and the corresponding surface areas of the catalysts were obtained using the BET method.

2.2. CO Hydrogenation. Catalytic evaluation of the catalysts with the CO hydrogenation reaction was performed on a small-scale stainless steel unit. Operational conditions and procedures were selected based on the results from previous studies.[4,5,14,23,24,28] The gases used were the following: H_2 (commercial grade, for sample reduction), N_2 (commercial grade, for reactor purge), and 31.7% CO/64.3% H_2/4% He (feed gas for reaction). Helium was used as an internal standard to calculate the total CO conversions. These gases passed through filtering elements at room temperature to remove residual O_2 and water traces.

The fixed bed reactor was a vertical stainless steel tube with an approximately 1.5 cm i.d., a wall thickness of 2 mm, and a length of 15 cm. A stainless steel screen was placed 5 cm from the bottom of the reactor to hold the catalyst sample. The gas flow went from top to bottom. The thermocouple tip reached the center of the reactor. A mass of sample between 0.7 and 2 g was dried overnight at 383 K and then reduced after helium flow for ~5−10 min to purge air from the reactor. Hydrogen flow for catalyst reduction was 30 mL min^{-1}. The oven temperature programmer was set to heat from room temperature to the chosen reduction temperature (573 or 773 K) at a slow rate of 2 K min^{-1}. The final temperature was maintained for 16 h. Immediately after the reduction, the reactor was purged with He at the reduction temperature for ~5−10 min and then cooled under He flow to the reaction temperature (543 K). The reaction was performed at atmospheric pressure and started after the temperature had stabilized by the CO/H_2/He mixture flow into the reactor at a rate of 10−20 mL min^{-1} to ensure constant space velocity for all experiments. The conditions were established for isoconversion around 5−10%. The total reaction time was approximately 50 h.

Reaction products were analyzed online with two gas chromatographs in series: first through a VARIAN-STAR3400 equipped with a flame ionization detector and then through a thermal conductivity detector (TCD). A Megabore HP-1 column was installed on the VARIAN-STAR3400 (methyl-silicone; 0.53 mm diameter; 30 m length; oven operated from 258 to 523 K at 5 K min^{-1} for each analysis; initial temperature was kept constant for 3 min). The TCD had a Porapak Q packed column, 3.18 mm ($^1/_8$ in.) in diameter and 9 m long (oven operated at constant temperature, 383 K). After the reactor, the tubing lines were kept at ~503 K to avoid product condensation. This hot stream passed through a six-way injection valve that collected ~0.1 cm^3 of gas sample.

2.3. Characterizations. *Diffuse Reflectance Spectroscopy (DRS) UV−visible.* Diffuse reflectance spectra were recorded in the range of 200−900 nm using an UV−vis near infrared (NIR) spectrophotometer (Cary 5E, Varian) equipped with an integrating sphere (Harrick). The support (alumina, niobia) and Nb_2O_5/Al_2O_3 samples were used as reference for the Co/Al_2O_3, Co/Nb_2O_5, and $Co/Nb_2O_5/Al_2O_3$ samples, respectively.

The DRS spectra were recorded on both calcined and pretreated samples. Samples were pretreated in the chamber passing He flow at 5 K min^{-1} up to 423 K for 30 min and cooled to room temperature for analysis. Then, it was switched to 10% H_2/Ar flow (20 mL min^{-1}) for the reduction and heated to 573 or 773 K, kept there for 30 min, and cooled to room temperature (RT) for analysis.

Diffuse Reflectance Infrared Fourier Transform Spectroscopy (DRIFTS). A Fourier transform infrared (FTIR) spectometer (Nicolet, model Nexus 470) equipped with a DRIFTS (diffuse reflectance infrared Fourier transform spectroscopy) cell (Spectra-Tech) chamber for high temperature treatment and a ZnSe mirror assembly was used to study the CO + H_2 reaction at different temperatures. These experiments were carried out after in situ reduction with pure H_2 (99.99) at 30 mL min^{-1} at 10 K min^{-1} up to 773 K for 6 h and then purged with He for 30 min. Subsequently, the sample was cooled to the reaction temperature. A feed mixture of 1 CO:2 H_2 (32% CO, 64% H_2, 4% He) was introduced at 25 mL min^{-1}, under similar reaction conditions. All spectra were obtained after an average of 64 scans from 650 to 4000 cm^{-1}, with a resolution of 4 cm^{-1} in the presence of the gas-phase species. Each spectrum was referenced to the spectrum of the reduced sample.

X-ray Photoelectron Spectroscopy (XPS). The X-ray photoelectron spectra were obtained using Mg Kα ($h\nu = 1253.6$ eV) monochromatized radiation with a Perkin-Elmer 1257 spectrometer. The spectra were analyzed in terms of relative peak area intensity and chemical shifts of the Co_{2p}, Nb_{2p}, and Al_{2p}. The charging effects were corrected using the C_{1s} peak, which was fixed on all the samples at a binding energy (BE) at 284.6 eV. The surface composition was determined by measuring the peak area intensities of the Nb_{3p} and Co_{3p}. The catalysts were

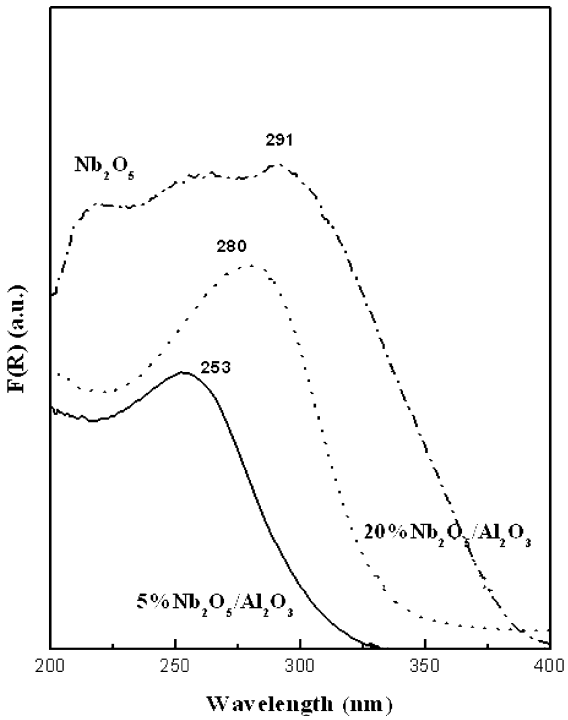

Figure 1. DRS of the $x\%Nb_2O_5/Al_2O_3$.

priori calcined and pretreated in the pretreatment chamber before analysis in the ultrahigh vacuum (UHV) chamber at 10^{-10} mbar.

Temperature-Programmed Reaction (TPR). The temperature-programmed reaction was performed in the same microreactor system; however, samples were collected in a multiloop valve (VCI-Valco) at different temperatures during heating, and at the end, all samples were analyzed online in a TCD chromatograph (Varian-STAR 3400). The catalyst (0.5 g) was previously reduced with pure hydrogen at 573 or 773 K during 16 h and then cooled to room temperature. Then, the catalysst was switched to the reaction mixture $H_2/CO = 2$ flowing at 30 mL min^{-1} and the temperature was raised at a heating rate of 20 K min^{-1} up to 773 K. Products were analyzed using a Porapak Q column under specific conditions: He flow (20 mL min^{-1}) at 323 K for 20 min and then heating, raising the temperature at 20 K min^{-1} up to 443 K.

3. Results

3.1. DRS Results. Figure 1 displays the DRS spectra of bulk Nb_2O_5 and of the $x\%Nb_2O_5/Al_2O_3$ samples. The alumina support was used as reference. The $5\%Nb_2O_5/Al_2O_3$ shows the d−d transition bands at 253 nm that with increasing niobia concentration are shifted to higher wavelengths and in the direction of the bulk sample (291 nm).

On the other hand, DRS spectra of the reduced Co-supported Co/Al_2O_3, $Co/5\%Nb_2O_5/Al_2O_3$, and Co/Nb_2O_5 catalysts are displayed in Figures 2, 3, and 4, respectively, showing different line shapes.

First of all, the Co/Al_2O_3 spectrum of the calcined sample (Figure 2) presented two strong absorption bands at 402 and 700 nm and a shoulder at 458 nm. These bands (402 and 700 nm) are attributed to Co^{3+} species in octahedral coordination,[29] whereas the shoulder (458 nm) is assigned to the octahedral Co^{2+} species.[30] After reduction at 573 K, it displays the same profile but is completely modified after reduction at 773 K (solid line), where cobalt species were partially reduced; however, the band around 300 nm remains. According to the literature,[31,32]

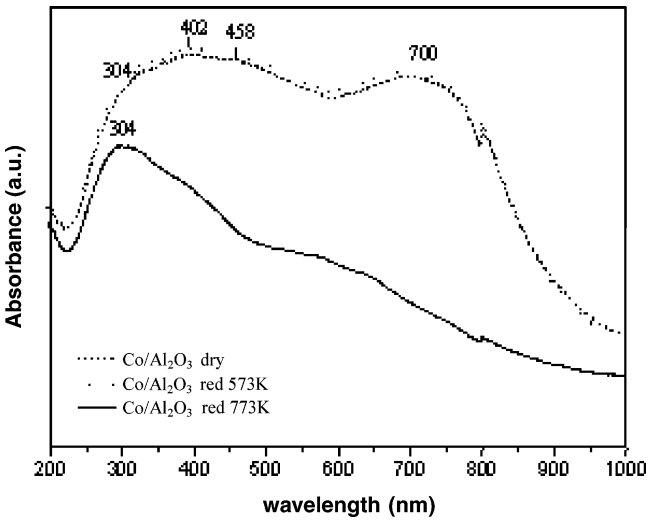

Figure 2. DRS spectra of the Co/Al_2O_3 catalyst after calcination and reduction at 573 and 773 K.

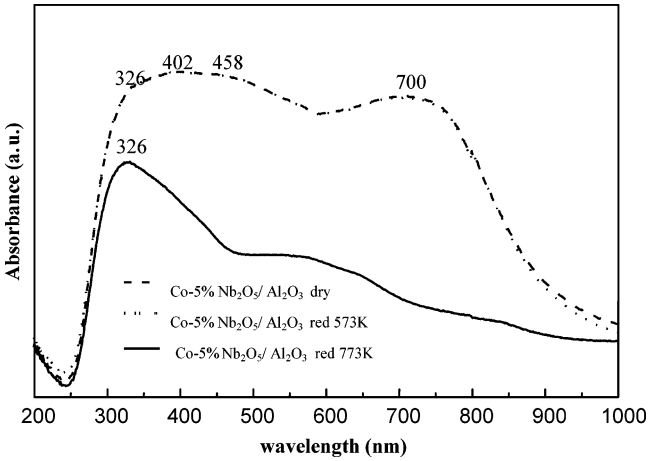

Figure 3. DRS spectra of the $Co/5\%Nb_2O_5/Al_2O_3$ catalyst after calcination and reduction at 573 and 773 K.

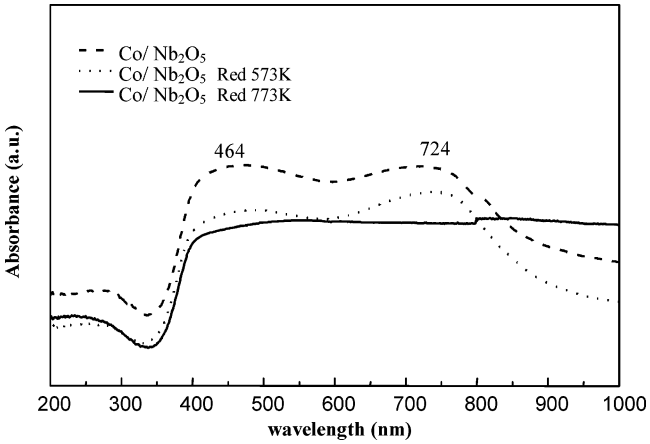

Figure 4. DRS spectra of the Co/Nb_2O_5 catalyst after calcination and reduction at 573 and 773 K.

this band could be assigned to tetrahedral Co^{2+} species. The spectral features of the $Co/5\%Nb_2O_5/Al_2O_3$ catalyst were similar to those of the Co/Al_2O_3 catalyst.

DRS spectra of 5% Co/Nb_2O_5 exhibited bands at 464 and 724 nm, which according to Noronha et al.[33] could be attributed to octahedral Co^{3+} and Co^{2+} species.

Figure 5 presents the absorbance spectra of all samples after reduction at 773 K. The addition of niobia shifted the band at

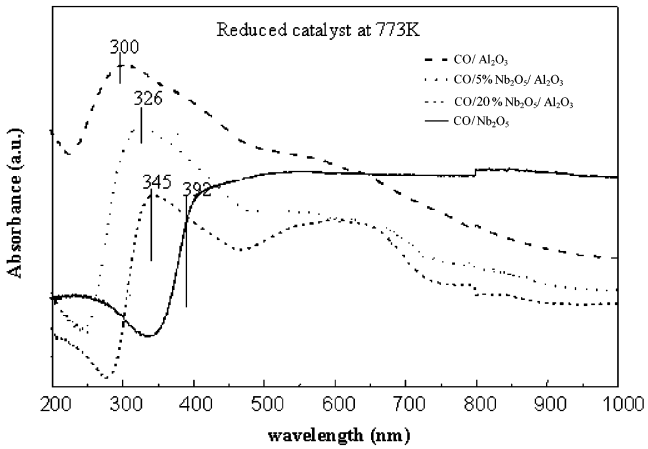

Figure 5. DRS spectra of all prepared catalysts after reduction at 773 K.

300 nm toward higher wavelength, compared to the Co/Al_2O_3 catalyst, while the intense band at 400 nm decreased with an increasing amount of niobia. However, it is worth noticing that the band at 300 nm was not observed for the Co/Nb_2O_5 catalyst, indicating surface cobalt species in intimate contact with the alumina support.

3.2. DRIFTS Results. Typical spectra of the samples 5% $Co/5\%Nb_2O_5/Al_2O_5$ and 5% $Co/20\%Nb_2O_5/Al_2O_5$ are displayed in Figure 6A and B, respectively. After in situ reduction with H_2, the $CO/H_2/He$ flow mixture was introduced at a ratio of $H_2/CO = 2$ during 6 h. The reference spectrum was the reduced catalyst prior to gas admission. Spectra were obtained at different temperatures. Figure 6A $Co/5\%Nb_2O_5/Al_2O_3$: (a) alumina at 473 K, (b) catalyst at 523 K, (c) catalyst at 543 K, (d) 523 K closed chamber/30 min, (e) 543 K closed chamber for 5 min. Figure 6B $Co/20\%Nb_2O_5/Al_2O_3$: (f) 473 K, (g) 523 K, (h) 543 K, (i) 523 K closed chamber/30 min, (j) 543 K closed chamber/30 min in flow system and after that in a closed chamber for 30 min of exposition and evacuation.

Figure 6A presents the spectrum of Al_2O_3 (spectrum a) under similar reaction conditions and were used with the reference spectrum. At 473 K, it displays characteristic bands of CO in the gas phase (2176 cm^{-1})[7,35,43] and formate species at 2902 cm^{-1} (νC−H), 1592 cm^{-1} (ν_{ass} C−O), 1393 cm^{-1} (δ_s C−H), and 1371 cm^{-1} (ν_s C−O).[44,45]

The $Co/5\%Nb_2O_5/Al_2O_3$ catalyst shows CO bands at different temperatures, 523 and 543 K (spetra b and c), indicating linear adsorption on top of metallic Co particles (2063 cm^{-1}). On the other hand, the band at 2060 cm^{-1} is attributed to the CO adsorption on $Co^{\delta+}$ species.[35] Zhang et al.[7] suggest the presence of ionic $Co^{\delta+}$ species with less electron donation capacity. With increasing temperature (523−543 K), this band is shifted toward 2039 cm^{-1}, suggesting an increase of reduced Co species.

Formate bands were observed at 2902 cm^{-1} (νC−H), 1592 cm^{-1} (ν_{ass} C−O), 1393 cm^{-1} (δ_s C−H), and 1371 cm^{-1} (ν_s C−O)[34,44,45] that increased with the temperature increase. Above 543 K, the band at 2354 cm^{-1}, relative to CO_2 formation was observed, which may be related to the "shift" reaction or/and the decomposition of formate species. The shoulder at 1650 cm^{-1} is assigned to the formation of −C═C−, suggesting the formation of olefins.

On the other hand, bands around 3000−2800 cm^{-1} evidence the presence of CH_x species during the reaction, suggesting also the formation of hydrocarbons, in particular the band at 3010

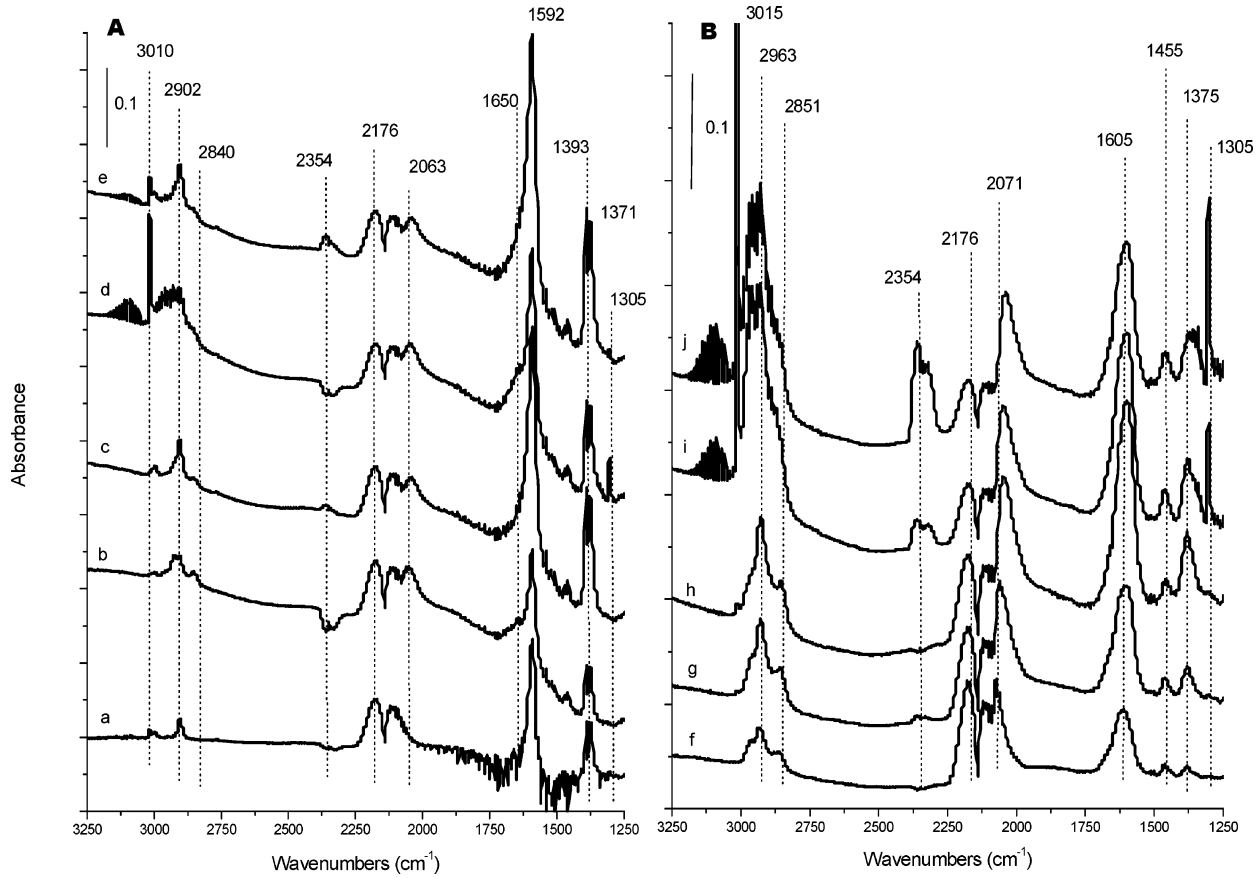

Figure 6. DRIFT spectra of the $CO/H_2/He$ mixture on catalysts. (A) $Co/5\%Nb_2O_5/Al_2O_3$: (a) alumina at 473 K, (b) catalyst at 523 K, (c) catalyst at 543 K, (d) 523 K closed chamber/30 min, (e) 543 K closed chamber for 5 min. (B) $Co/20\%Nb_2O_5/Al_2O_3$: (f) 473 K, (g) 523 K, (h) 543 K, (i) 523 K closed chamber/30 min, (j) 543 K closed chamber/30 min.

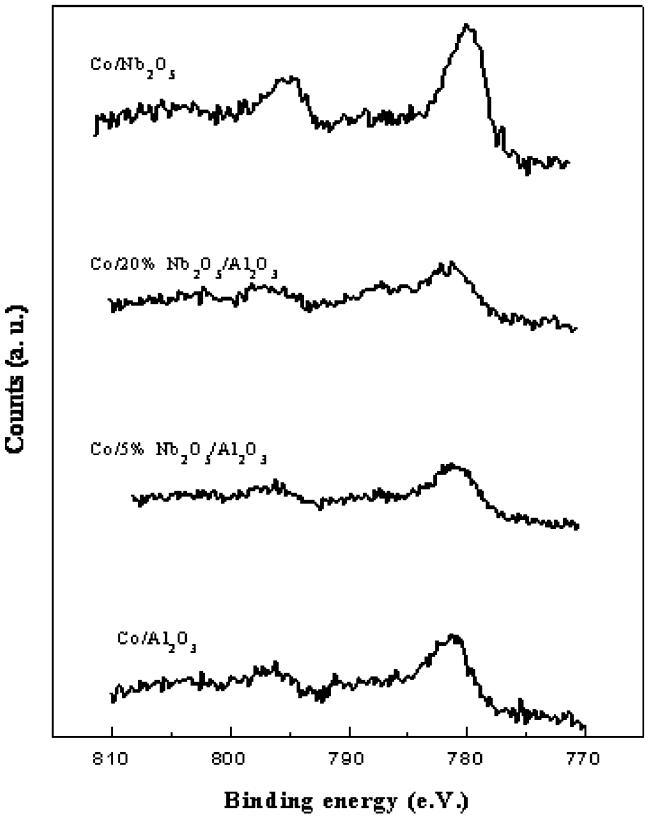

Figure 7. XPS of $Co/x\%Nb_2O_5/Al_2O_3$ precursors.

cm^{-1}, which corresponds to axial deformation, and that at 1305 cm^{-1}, corresponding to the angular deformation of the C−H bond of the gas methane. According to Rygh et al.,[35] these bands are due to the formation of intermediate CH_x species.

The $Co/5\%Nb_2O_5/Al_2O_3$ catalyst displays the symmetric stretching of $-CH_2$ at 2840 cm^{-1}, that evidences this intermediate species. Spectra d and e confirm these bands taken in a closed chamber after evacuation.

The $Co/20\%Nb_2O_5/Al_2O_3$ (Figure 6B) displays similar behavior for CO adsorption on $Co^{\delta+}$ species (∼2070 cm^{-1}), that changes with increasing temperatures. However, significant modifications were observed between 3000 and 2800 cm^{-1} and 1650−1250 cm^{-1}. One can see that the formation of CH_x intermediates at 523 K, related to the bands at 2951 cm^{-1} (ν_s CH_2), 2928 cm^{-1} (ν_{ass} CH_2), and 2963 cm^{-1} (ν_{ass} CH_3), and the band at 3015 cm^{-1} related to the CH_4 gas; while at 1455 cm^{-1} (δ_{ass} CH_2+CH_3) and 1375 cm^{-1} (δ_s CH_3) and at 1305 cm^{-1} (δ C−H), there are bands related to methane. The band at 1605 cm^{-1} (ν C═O) is due to the adsorption of bidentade carbonate species, which are responsible for CO_2 formation. The identification of formate species (∼1590 cm^{-1}) is not so evident, because this band can superpose the band 1605 cm^{-1}. Moreover, the band at 2902 cm^{-1} was not observed as before and is attributed to the axial deformation of the C−H bonding of formate. The presence of carbonates and absence or small formation of formate indicate the influence of the niobia content in the catalyst.

3.3. X-ray Photoelectron Spectroscopy. XPS spectra of the calcined precursors $Co/x\%Nb_2O_5/Al_2O_3$, Co/Nb_2O_5, and Co/Al_2O_3 are shown in Figure 7. Table 2 presents the binding energy of all studied systems, while Table 3 contains the spin−orbital coupling values as well as the relative intensities between the satellite peaks and the principal peak of the precursors. Co/Nb_2O_5 displays a binding energy of 780.0 eV for $Co2p_{3/2}$ (Table 2), without a satellite peak and a spin−orbital coupling of 15.4 (Table 3). The calcined precursor of Co/Al_2O_3 displays a binding energy of 781.4 eV for $Co2p_{3/2}$ and a spin−orbital coupling of 14.80 with a small satellite relative intensity peak to the $Co2p_{3/2}$ of 0.334. For the $Co/x\%Nb_2O_5/Al_2O_3$ precursors, the addition of niobia does not change this ratio noticeably.

TABLE 2: Binding Energy of Cobalt-Supported Catalysts

catalysts	$Co2p_{1/2}$	$Co2p_{3/2}$ (eV)	O1s (eV)	$Nb3d_{5/2}$ (eV)	$Nb3d_{3/2}$ (eV)	Al2p (eV)
Co/Al_2O_3	796.2	781.4	531.6			74.4
$Co/5\%Nb_2O_5/Al_2O_3$	796.2	781.2	531.4	207.2	210	74.4
$Co/20\%Nb_2O_5/Al_2O_3$	798.2	781.8	531.4	207.6	210.2	74.6
Co/Nb_2O_5	795.4	780.0	530.2	207.0	209.6	
Co_3O_4	795.4	780.4	530.0			
niobate	797.2	781.2	534.0	206.8	209.6	
aluminate	797.2	781.6	531.2			74.0

3.4. CO Hydrogenation. Table 4 presents the product distribution of the CO hydrogenation at 543 K for all catalysts reduced at different temperatures for 24 h on stream. These results were obtained at isoconversion. The Co/Al_2O_3 catalysts reduced at 573 and 773 K presented similar selectivities: high selectivity to methane (45−53.2%), light hydrocarbons (34−31.5%), and a low fraction of higher chain carbon hydrocarbons C_5^+ (17−10.6%). The Co/Nb_2O_5 catalyst reduced at 573 K was also similar to Co/Al_2O_3 (CH_4 = 56.2% and C_5^+ = 14.8%). However, a considerable change was observed when the same catalyst was reduced at 773 K. The CH_4 selectivity was 5 times lower, with a significant increase of C_5^+, mainly indicating the formation of linear hydrocarbons in the gasoline and diesel fraction. On coating niobia over alumina catalysts ($Co/x\%Nb_2O_5/Al_2O_3$) reduced at 573 K, the results were not significantly different as compared with those of the Co/Al_2O_3 catalyst. However, with higher niobia loading and, in particular, after reduction at 773 K (see $Co/20\%Nb_2O_5/Al_2O_3$), those systems behaved like the monometallic Co/Nb_2O_5 catalyst; although less active, methane was low and C_5^+ selectivity was higher as well.

Table 5 collects the reaction rates for different reduction temperatures, including, for comparison, our previous results.[14] On the basis of these results, we observed that the activity decreases as follows: Co/Al_2O_3 > Co/Nb_2O_5 > $Co/20\%Nb_2O_5/Al_2O_3$.

The TPSR profiles for methane formation are shown in Figure 8, displaying the molar fraction of methane as a function of the reaction temperature. The Co/Al_2O_3 reduced at 573 K shows an increase of methane with increasing temperature, while when reduced at 773 K the formation of methane reaches a maximum around 630 K, which could be attributed either to coke formation or sintering.

On the other hand, the Co/Nb_2O_5 catalyst exhibited two peaks after reduction at 573 K, with a maximum around 575 and 750 K, while the catalyst reduced at 773 K, although less active, shifted the first peak to a lower temperature. In both cases, the maximum of the second peak was shifted to higher temperatures compared to the Co/Al_2O_3 catalyst.

4. Discussion

Figure 1 shows the DRS spectra of the Nb_2O_5 and Nb_2O_5/Al_2O_3 samples. All Nb_2O_5/Al_2O_3 samples exhibited a metal−ligand charge transfer band. This band was shifted to higher wavelength as the niobium content increased. Tanaka et al.[37] have already discussed the transition bands of supported niobium oxides and claimed that they are dependent on the degree of polymerization of surface ions, suggesting an increasing degree of polymerization of niobium species. According to the authors,

TABLE 3: Atomic Ratios, Spin−Orbital Coupling, Rationed Satellite Peaks, and Main Peak of Calcined Precursors

sample	fraction of surface Co[a] (XPS)	fraction of bulk Co[a]	I_{Nb}/I_{Al} XPS	I_{Nb}/I_{Al} bulk	ΔE[b]	R[c]
Co/Al_2O_3	0.0110	0.0180			14.80	0.3340
$Co/5\%Nb_2O_5/Al_2O_3$	0.0180	0.0180	0.0865	0.0213	15.00	0.3706
$Co/20\%Nb_2O_5/Al_2O_3$	0.0240	0.0200	0.1578	0.1023	16.40	0.5820
Co/Nb_2O_5	0.0300	0.0340			15.40	0.2305
Co_3O_4					15.00	0.1723
niobate					16.00	0.5103
aluminate					15.60	0.4699

[a] $I_{CO}/(I_{CO} + I_{Al} + I_{Nb})$, where I_i is the intensity signal of CO, Al, and Nb. [b] ΔE = distance between lines $Co2p_{3/2}$ and $Co2p_{1/2}$ (spin−orbital). [c] R = ratio between satellite peak and line of $Co2p_{3/2}$.

TABLE 4: Selectivity to Methane (CH_4), Hydrocarbons (C_2-C_4), Gasoline (C_5-C_{12}), Diesel ($C_{13}-C_{18}$), and Fractions above (C_{19}^+)[a]

catalysts	T_{red} (K)	CH_4	light HC	gas[b]	diesel	C_{19}^+	alcohol	C_5^+[c]
Co/Al_2O_3	573	45.0	34.0	13.6	2.6	1.2	3.4	17.0
	773	53.2	31.5	9.2	1.9	0.2	3.9	10.6
$Co/5\%Nb_2O_5/Al_2O_3$	573	53.4	32.7	9.0	0.9	0.1	3.9	10.0
	773	50.4	33.8	10.5	0.9	0.05	4.3	11.5
$Co/20\%Nb_2O_5/Al_2O_3$	573	50.1	30.1	9.3	5.2	0.4	4.8	14.9
	773	41.8	30.5	14.0	8.2	2.2	3.2	24.4
Co/Nb_2O_5	573	56.2	24.9	10.8	3.8	0.2	5.1	14.8
	773	10.3	29.0	33.8	18.8	2.3	5.8	55.0

[a] Conversions: 5−10%. [b] gas = gasoline. [c] $C_5^+ = \sum(C_5...C_{13}) + (C_{13}...C_{18})$ and C_{19}^+.

TABLE 5: Influence of the Reduction Temperature and Nb_2O_5 Content on the Reaction Rate of CO[a]

catalysts	T_{red} (K)	conversion (%)	rate CO[b] (μmol s^{-1} g cat^{-1})	ratio R_{CNbAl}/R_{CAl}
Co/Al_2O_3	573	12.2	2.13	1.0
	773	10.9	2.30	1.07
$Co/5\%Nb_2O_5/Al_2O_3$	573	13.7	1.50	0.70
	773	14.3	1.56	0.73
$Co/20\%Nb_2O_5/Al_2O_3$	573	10.9	1.20	0.56
	773	10.9	1.10	0.51
Co/Nb_2O_5	573	13.0	1.42	0.66
	773	3.8	0.05	0.023

[a] Ratio $H_2/CO = 2$; $P = 1$ atm; $T_{reaction} = 543$ K. [b] Reaction rate after stabilization for 24 h (μmol s^{-1} g cat^{-1}).

the samples containing low niobium oxide loading have monomeric and oligomeric NbO_4 tetrahedra species, whereas the high loading catalysts contain Nb_2O_5 particles. Therefore, it is possible to infer a polymeric formation of intermediate niobium species with increasing niobium content, that are the precursors of the bulk niobium oxide (Nb_2O_5), exhibiting a d−d band at 291 nm. Indeed, the d−d bands of the intermediate species are 253, 280, and 291 nm for 5, 20, and 100% of niobium contents, respectively (see Figure 1).

Concerning the Co-supported catalysts, we have analyzed the TPR results of these catalysts, which have shown different reduction peaks for Co/Al_2O_3, changing with increasing Nb_2O_5 content, as reported previously.[43] The total H_2 consumptions are presented in Table 1, and it can be seen that the reduction is not complete. The total H_2 consumption for the complete reduction of Co_3O_4 to metallic Co^0 is 1.17 μmol g cat^{-1}. The excess of H_2 for the Co/Nb_2O_5 catalyst is due to the reduction of Nb_2O_5 at the surface.

There are three different cobalt species identified in the Co/Al_2O_3 catalyst: Co_3O_4 particles, Co^{2+} species, and a spinel structure of $CoAl_2O_4$,[37,38] which occurs at higher temperature

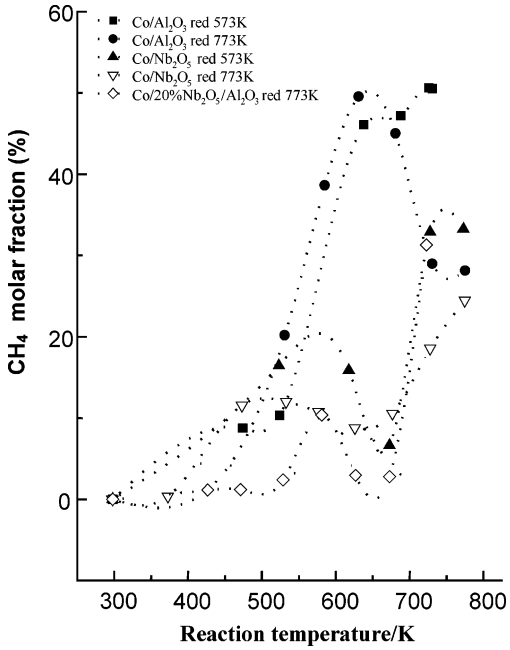

Figure 8. TPSR plot of methane formation with reaction temperature of the catalysts reduced at 573 and 773 K.

and is related to the reduction of surface Co^{2+} species with strong interaction with the alumina support. The reduction of Co_3O_4 to Co^0 corresponds to only 33%.

The Co/Nb_2O_5 presents different degrees of reduction at different temperatures: reduction of Co_3O_4 to Co^0, partial reduction of Co^{2+} species, and partial reduction of the support at elevated temperatures, which correspond to an H_2 consumption of 135%, indicating reduction of Nb^{5+} in contact with Co particles at the surface. On the other hand, the $Co/20\%Nb_2O_5/Al_2O_3$ sample shows only one reduction peak, corresponding to a reduction of 59% of the Co_3O_4 to Co^0, leaving Co^{2+} species at the surface in contact with niobia. In this case, it seems that at least 40% of the Co^{2+} remain as surface species.

These results are in agreement with the DRS and XPS findings, relative to the presence of Co^{2+} species at the surface, regarding niobate compounds such as $Co_2Nb_5O_{14}$ and of $CoNb_2O_6$, which can be reduced at elevated temperatures to metallic cobalt. For higher temperatures, the reduction of NbO_2 particles was also observed.[15]

In fact, DRS results of the Co-supported calcined samples exhibited bands, which can be attributed to Co^{3+} in octahedral coordination and octahedral Co^{2+} species, in agreement with Ashley and Mitchell.[32] DRS spectra of the catalysts containing 5 and 20 wt % Nb_2O_5 show broader bands, but the spectral features were similar to those of the Co/Al_2O_3 catalyst. DRS spectra of $5\%Co/Nb_2O_5$ exhibited bands at 464 and 724 nm, which are attributed to octahedral $Co^{3+}$and Co^{2+} species.

Figure 3 shows the DRS absorbance spectra of the $Co/5\%Nb_2O_5/Al_2O_3$ catalysts after reduction in situ at 573 and 773

K. It appears that at 573 K the cobalt species did not change, exhibiting the same profiles and suggesting that little metallic cobalt is present at the surface, the cobalt ions Co^{3+} and Co^{2+} being the prevailing species. However, after reduction at 773 K, the DRS profile was different, indicating that beside the reduction of cobalt oxide the cobalt species were partially reduced, as seen by the band at 300 nm (Figure 5), which is assigned to tetrahedral Co^{2+} species[21,31] and still remains after the reduction treatment. These results suggest that the amount of cobalt species which are in contact with the support affect the intensity bands and therefore the coordination of Co species. Thus, the in situ DRS results reinforce qualitatively the presence of metallic cobalt and cobalt species ($Co^{\delta+}$), which are dependent on the degree of reduction and the degree of the contact between cobalt and the support or the intermediate niobium species over the support.

For complementing the identification of $Co^{\delta+}$ species, XPS line shapes of Co2p were taken for Co_3O_4, aluminate, and niobate compounds and could not be distinguished alone through the binding energy of Co2p.[33] Secondary aspects, such as the relative intensity of satellite peaks (*R*) and spin−orbital coupling (ΔE between lines $Co2p_{3/2}$ and $Co2p_{1/2}$) have to be taken in account (Table 3). The binding energy of $Co2p_{3/2}$ of Co_3O_4 is 780.4 eV without a satellite peak, while niobate, aluminate, and CoO present a satellite peak. The spin−orbit coupling of Co_3O_4 is around 15.0, but it is larger for Co^{2+} (CoO = 16.0, niobate = 16.0, and an intermediate value for aluminate = 15.6).[33]

Both Co/Al_2O_3 and Co/Nb_2O_5 present spin−orbit splitting values close to those of Co_3O_4. However, the precursor containing 20% Nb_2O_5 gives rise to higher values.

A comparison between the Co/Al_2O_3 catalyst and the compound references suggests that most particles consist of Co_3O_4, because ΔE and *R* are consistent with the value of this compound. According to the literature,[33] for the calcined 5%Co/Nb_2O_5 precursor, the binding energy for $Co2p_{3/2}$ is 780.3 eV and spin−orbit splitting is 15.4, which are close to our findings and suggest that Co_3O_4 particles are prevailing at the surface.

The $Co/Nb_2O_5/Al_2O_3$ systems show an increase of 0.7 eV in the spin−orbit splitting coupling value and suggest an increase of Co^{2+} species. The calcined precursor $Co/20\%Nb_2O_5/Al_2O_3$ shows significant increase of the satellite peak and spin−orbital values.

4.1. Reactivity and Selectivity. The dispersions were obtained by H_2 chemisorption measurements (not shown). The dispersions on the Co/Al_2O_3 catalyst reduced at 573 and 773 K are very low, 12 and 6.7%, respectively, and based on the irreversible adsorption at 448 K, suggesting the presence of big cobalt particles; however, for higher reduction temperatures, the particles become even larger due to sintering. The dispersions of the Co/Nb_2O_5 are lower than those for Co/Al_2O_3 and, in particular, for a temperature of reduction of 773 K, where the dispersion is even much lower, 9.3% at 573 K and 4.8% at 773 K, respectively. This is not surprising, has already been observed for reducible supports, such as TiO_2 and Nb_2O_5, and has been attributed to the SMSI effect, due to the migration of reduced Nb_2O_x patches over the cobalt particles.[14,27,38,39] Measurements of metallic cobalt dispersion onto an Nb_2O_5 surface are imprecise due to the reduction of Nb^{5+} in contact with metallic Co^0 at the surface, which makes the determination of the activity based on the metallic dispersion difficult. Therefore, one can calculate the relative activity of the different catalysts, using, as a reference, the rate of CO production (*R*) (μmol s^{-1} g cat^{-1}) of the Co/Al_2O_3 catalyst reduced at 573 K, as shown in Table 5 for different reduction temperatures. The activity of Co/Al_2O_3 is practically equal for both reduction temperatures at 573 and 773 K; however, it was 30% lower for the $Co/5\%Nb_2O_5/Al_2O_3$ catalyst but approximately equal for both reduction temperatures at 573 and 773 K. With increasing Nb_2O_5 content and with a pure Nb_2O_5 support, the activity of $Co/20\%Nb_2O_5/Al_2O_3$ and Co/Nb_2O_5 catalysts decreased around 40% compared to the Co/Al_2O_3 catalyst but was approximately equal for both reduction temperatures, with the exception of the Co/Nb_2O_5 catalyst reduced at 773 K. These results suggest that the addition of Nb_2O_5 anchored on alumina reduced the metallic sites, which, indeed, indicate the formation of larger particles and therefore lower dispersions, independent of the temperature of reduction. However, the activity of the Co/Nb_2O_5 catalyst reduced at 773 K was very low, which is in accordance with the low dispersion of cobalt compared to the other ones, indicating besides larger particles the presence of an SMSI effect due to the formation of NbO_x patches and their migration of the cobalt particles. In conclusion, the activity depends on the niobia content anchored on alumina; however, for a pure Co/Nb_2O_5 catalyst reduced at 773 K, the SMSI effect prevails. The activity depends mainly on the metallic Co^0 particle sizes at the surface.

Table 4 presents the selectivity of the different products, and remarkable differences were observed depending on the reduction temperature, which indeed reflects the changes of the surface active sites.

The TPSR profiles of methane formation, as shown in Figure 8, display the molar fraction of methane as a function of the temperature. While the monometallic catalysts present one peak, the $Co/x\%Nb_2O_5/Al_2O_3$ catalyst exhibits at least two peaks after reduction at 573 and 773 K, where the first peak is shifted to a lower temperature and the second peak shifted to higher temperatures after reduction at 773 K. These curves evidence a transient behavior of the reaction, which depends on the reduction temperature. Similar observations were observed for other systems and could be explained through different reaction mechanisms due to the formation of different surface sites.

Lee and Bartholomew[40] observed two peaks of methane formation for the Co/Al_2O_3 catalyst using the TPSR technique. They attributed the formation of the low temperature methane peak to methane formed on big metallic Co^0 crystallites, and the second peak they considered to indicate a methane formation through CH_xO species that had been formed on the support, due to spillover, followed by decomposition of these species on metallic particles, due to back spillover.

However, such oxygenate species would also depend on the nature of the surface of the support. In the case of alumina, probably, such a spillover effect could be explained by the caption of oxygen from the hydroxyl groups. On the basis of the dispersion, there are big Co particles apparently covering the external surface of alumina, which probably hamper the spillover of such species through the support. The surface area of the niobia support is much smaller than the one of alumina, and therefore, there are big cobalt particles covering the external surface of the support too. However, the question is what kind of species are there. The DRS and XPS results presented above evidence the presence of Co^{3+} and Co^{2+} species on the surface of the niobia support, in accordance with the literature.[17,23] Metallic Co^0 coexists with Co^{2+} species after reduction, and the majority of Co^0 originate from Co_3O_4, which can be transformed partially into Co^{2+} and subsequently into Co^0 in addition to a thin layer of Co^{2+} species, which still remains after calcination.[17] These Co^{2+} species are strongly interacting with the support, are distributed as a thin layer at the surface, and, hence, are very difficult to reduce to metallic cobalt, but

only at elevated temperature, as reported previously.[17,23] It was observed by DRS in situ that a majority of Co^{2+} species exist after reduction at 573 K, but for 773 K, these surface species are then reduced to metallic cobalt (Figures 4 and 5).

DRIFTS experiments on a typical $Co/x\%Nb_2O_5/Al_2O_3$ catalyst showed CO adsorption on metallic Co^0 at 2119 cm^{-1}. According to Toomes and King,[42] this band corresponds to CO adsorption on top of metallic cobalt (2130 cm^{-1}). Moreover, Jiang et al.[41] observed one band at 2080 cm^{-1}, which was taken as an indication of CO adsorbed on $Co^{\delta+}$ ($0 < \delta < 2$). In addition, Rygh et al.[35] attributed the band at 2060 cm^{-1} to overlapping bands from $Co(CO)_n$ and $Co^{\delta+}-CO$ on a single crystal.

A new band appeared at 2170 cm^{-1} even at room temperature and was unperturbed at high temperatures. It has not been reported before for Co-supported systems. Freund et al.[36] attributed this band to the stretching vibration frequency of CO adsorbed on a hydroxylated CoO(111)/OH surface.

On the other hand, CH_xO formate species are also displayed at 2902 cm^{-1} in the DRIFTS experiments of the sample reduced at 773 K, corresponding to the CH stretching of adsorbed formate ions. Marked differences were observed during DRIFTS experiments fluxing CO and H_2, displaying the formation of new bands at 1650, 1592, 1393, and 1371 cm^{-1}. The band at 1647 cm^{-1} appeared at 473 K and disappeared at 543 K, which indicates the presence of an olefin $-C=C-$ at the surface. On the other hand, the bands at 1592, 1393, and 1371 cm^{-1} increased with increasing temperature, which is an indication of the formation of $-CH_n-$ fragments or geminate CH_3 groups. Other bands did not change with increasing reaction temperatures. All this suggests the formation of linear chain growth at the surface of the catalysts studied. In addition, CO hydrogenation on these catalysts reveals the prevailing presence of linear hydrocarbons (paraffins).

Rygh et al.[35] confirmed Lee's proposals, indicating that CO is dissociated on large metallic crystallites followed by hydrogenation of the α-carbon and a spillover of CO and H to the support with the formation of CH_xO complexes, which, in the following, diffuse back to the metal and decompose. They also claim that the H spillover promotes the reduction of Co species.

Therefore, our results suggest likewise that the CH_xO species are the precursors for the formation of hydrocarbons, and characterizations revealed the presence of Co^0 particles (big particles because of the low dispersion) which are surrounded by Co^{2+} species. CH_x^- is thought to be formed as methyl radicals on Co^0 particles, as displayed by DRIFTS. The methyl radicals might migrate toward Co^{2+} with the caption of oxygen atoms from CoO allowing for the formation of intermediate CH_xO complexes, followed by decomposition to methane on metallic Co^0 particles. With an increasing temperature of reduction, Co^{2+} species can be reduced to Co^0, and therefore, the back spillover may occur on these new interfaces (Co^0-Co^{2+}), which increase during the reaction, allowing decomposition to methane on the metallic sites. Indeed, DRS results showed bands at 402 and 700 nm, which are attributed to Co^{3+} in octahedral coordination, and a shoulder around 458 nm, which corresponds to the octahedral Co^{2+} species, in addition to the band around 300 nm that remains after the reduction and is attributed to tetrahedral Co^{2+} species.

DRIFTS results displayed also growing amounts of CH_3 groups. It is noteworthy that the niobium intermediates facilitate the formation of such interfaces, probably due to the formation of NbO_x complexes. It explains why chain growth is facilitated in the presence of these complexes, disfavoring methane formation and favoring selectivity toward higher hydrocarbon formation. The lower the methane production is, the higher the presence of long chain hydrocarbons.

Finally, the TPR results on the Co/Nb_2O_5 reported previously[43] showed that after an initial reaction at lower temperatures the catalysts suffers deactivation and then experiences an activation process, which can be explained by the SMSI effect and not by coke formation. The XPS intensity ratio (I_{Nb}/I_{Al}) in Table 3 indicates a high concentration of Nb at the surface, and TPR results evidence the reduction of Nb_2O_5 at the surface. Indeed, NbO_x species present at the interface migrate over Co^0 with the formation of patches, blocking metallic surface sites. However, with the formation of water during the reaction, as reported by Kunimori et al.[38] and Haller and Resasco,[39] the surface is cleaned up and the NbO_x species are partially removed from the metallic Co^0 surface. It seems that during this process formation and destruction of new interfaces involving Co^0-NbO_x sites occur. DRIFTS and selectivity results suggest that these sites might be responsible for the reaction chain growth and therefore for the drastic change in the selectivity of CH_4 and C_5^+ hydrocarbons, mainly on the Co/Nb_2O_5 catalyst.

The catalyst containing 20 wt % Nb_2O_5 exhibited similar behavior, approaching monometallic when reduced at high temperature. DRS results of these catalysts showed bands shifted toward higher wavelength compared to the Co/Al_2O_3 catalyst. A band around 300 nm remained after the catalysts have been reduced at high temperature, which suggests the presence of cobalt oxide species at the alumina support, however, in smaller amounts compared to the Co/Nb_2O_5 catalyst itself.

These results allow us to suggest the formation of interfacial sites, such as Co^0-Co^{2+} sites and $Co^0-Nb_2O_x$ sites, leading to reaction pathways of two-site reactions: First, CO dissociates on Co^0 sites by forming α-carbon and, subsequently, methyl groups which spillover to the interfacial (Co^0-Co^{2+}) sites, leading to intermediary methoxy species formation. Second, in the presence of niobia, formation of methyl radicals at interfacial Co^0-NbO_x sites is suggested, which allows for chain growth, favoring the formation of higher than C_5^+ chains.

5. Conclusions

DRS and XPS results showed that NbO_x species are formed upon coating Nb_2O_5 over an alumina support, which grows like a polymer structure at the surface with increasing niobia loading until the formation of a monolayer is completed. Above 20% niobia loading, larger Nb_2O_5 particles were formed.

DRS results of Co niobia/alumina systems showed the presence of Co^{3+} and Co^{2+} species in different coordination environments. After reduction at 573 K, they are the prevailing species. When reduced at 773 K, the Co^{2+} or Co^{3+} species are partially reduced to Co^0, an effect which decreases with Nb loading.

Characterizations including DRS, XPS, DRIFTS, and selectivity results on $Co/x\%Nb_2O_5/Al_2O_3$ catalysts have shown that surface modification takes place via the formation of metallic Co^0, surface $Co^{\delta+}$ ions, and interfacial $Co^{\delta+}-NbO_x$ sites. It seems that during the reaction process formation and destruction of new interfaces occur, and results suggest that these sites might be responsible for the reaction chain growth and therefore for the drastic change in the selectivity of CH_4 and C_5^+ hydrocarbons, mainly on the Co/Nb_2O_5 catalyst.

DRIFTS results of $Co/Nb_2O_5/Al_2O_3$ catalyst showed olefins disappearing with an increasing temperature of reaction and simultaneously increasing formation of methyl radical groups and methoxy, which are the precursors of longer hydrocarbon chains.

The obtained results are in good agreement with our TPR results, which have been previously published. The activity relative to methane formation for $Co/Nb_2O_5/Al_2O_3$ was dependent on the reduction temperature. Catalytic results showed high C_1 and low C_5^+ formation for lower Nb contents but, on the other hand, extremely low C_1 and high C_5^+ with higher NbO_x loading, suggesting that in the first case Co^0-Co^{2+} are the active sites, while in the second case interfacial $Co-NbO_x$ and Co^0-Co^{2+} are the active sites.

References and Notes

(1) Mendes, F.; Noronha, F. B.; Soarez, R. R.; Perez, C. A. C.; Marcheti, G.; Schmal, M. *Stud. Surf. Sci. Catal.* **2001**, *136*, 177.

(2) Schulz, H. *Appl. Catal.* **1999**, *186*, 3.

(3) Bertole, J. C.; Mins, A. C.; Kiss, G. *J. Catal.* **2004**, *221*, 191.

(4) Mendes, F. T.; Noronha, F. B.; Schmal, M. *Stud. Surf. Sci. Catal.* **2000**, *130*, 3717.

(5) Mendes, F.; Noronha, F. B.; Soares, R. R.; Perez, C. A. C.; Marcheti, G.; Schmal, M. *Stud. Surf. Sci. Catal.* **2001**, *136*, 177.

(6) Martinez, A.; Lopez, C.; Márquez, F.; Díaz, I. *J. Catal*. **2003**, *220*, 486.

(7) Zhang, J.; Chen, J.; Ren, J.; Sun, Y. *Appl. Catal. A* **2003**, *243*, 121.

(8) Hachenberg, H.; Wunder, F.; Leupoid, E. I.; Schmidt, H. J. European patent application 21330, 1981.

(9) Kuznetsov, V. L.; Lisitsyn, A. S.; Golovin, A. V.; Aleksandrov, M. N.; Yermakov, Yu. I.; In *Homogeneous and Heterogeneous Catalysis*; Yermakov, Yu. I.; Likholobov, V., Eds.; VNU Science Press: Utrecht, The Netherlands, 1986.

(10) Lisitsyn, A. S. Golovin, A. V.; Chuvilin, A. L.; Kuznetsov, V. L.; Romanenko, A. V.; Danilyuk, A. F.; Yermakov, Yu. I. *Appl. Catal.* **1989**, *55*, 235.

(11) Fujimoto, K.; Oba, T. *Appl. Catal*. **1985**, *51*, 289.

(12) Derule, H.; Blanchard, M.; Canesson, P. *Appl. Catal.* **1989**, *50*, L1.

(13) Schnke, D. D. *New Trends of Methane Activation*; Elsevier: New York, 1990.

(14) Silva, R. R. C. M.; Dalmon, J. A.; Frety, R.; Schmal, M. *J. Chem. Soc., Faraday Trans.* **1993**, *89* (21) 3975.

(15) Noronha, F. B.; Frydman, A.; Aranda, D. A. G.; Soares, R. R.; Moraweck, B.; Castner, D. D.; Campbell, C. T.; Frety, R.; Schmal, M. *Catal. Today* **1996**, *28*, 147.

(16) Sinfelt, J. H. *Bimetallic Catalysts Discoveries, Concepts and Applications*; Wiley: New York, 1983.

(17) Frydman, A.; Campbell, C. T.; Castner, D.; Schmal, M. *J. Catal.* **1995**, *157*, 133.

(18) Kapoor, M. P.; Lapidus, A. L.; Krylova, A. Y. In *Proceedings of the 10th International Congress on Catalysis*; Guczi, L., Solymosi, F., Tetenyi, P., Eds.; Elsevier: Budapest, 1992; Part C, p 2741.

(19) Iglesia, E.; Soled, S. L.; Fiato, A.; Via, G. H. *J. Catal.* **1993**, *143*, 345.

(20) Iglesia, E. *Appl. Catal. A* **1997**, *121*, 59.

(21) Tsubaki, N.; Sun, S.; Fujimoto, K. *J. Catal.* **2001**, *199* 236.

(22) Macedo, J. C. D.; Schmal, M.; Dalmon, J. A. In *Proceedings of the X Symposium Iberoamerican on Catalysis*; 1986; Part 2, p 666.

(23) Frydman, A.; Soares, R. R.; Schmal, M. *Stud. Surf. Sci. Catal.* **1993**, *75*, 2796.

(24) Soares, R. R.; Frydman, A.; Schmal, M. *Catal. Today* **1983**, *16*, 361.

(25) Iizuka, T.; Tanaka, Y.; Tanabe, K. *J. Mol. Catal.* **1982**, *17*, 381.

(26) Vannice, M. A.; Garten, R. L. *J. Catal.* **1979**, *56*, 236.

(27) Ko, E. I.; Hupp, M. *J. Catal.* **1984**, *86*, 315.

(28) Dietz, W. A. *J. Gas Chromatogr*. **1967**, (February), 68.

(29) Sass, A. S.; Shvets, V. A.; Svelèva, G. A.; Kasanskii, U. B. *Kinet. Katal*. **1985**, *26* (5), 1149.

(30) Chung, K. S.; Massoth, F. E. *J. Catal*. **1980**, *64*, 320.

(31) Lever, A. B. P. *Inorganic Spectroscopy*; Elsevier: Amsterdam, 1968.

(32) Ashley, J. H.; Mitchell, P. C. H. *J. Chem. Soc. A* **1968**, 2821.

(33) Noronha, F. B.; Perez, C. A.; Schmal, M.; Fréty, R. *Phys. Chem. Chem. Phys.* **1999**, *1*, 2861.

(34) Busca, G.; Lamotte, J.; Lavalley, J. C.; Lorenzelli, V. *J. Am. Chem. Soc.* **1987**, *109*, 5197.

(35) Rygh, L. E. S.; Nielsen, C. J. *J. Catal.* **2000**, *194*, 401.

(36) Schonnenbeck, M.; Cappus, D.; Klinkmann, J.; Freund, H. J.; Petterson, L. G. M.; Bagus, P. S. *Surf. Sci.* **1996**, *347*, 337.

(37) Tanaka, T.; Nojima, H.; Yoshida, H.; Nakagawa, H.; Funabiki, T.; Yoshida, S. *Catal. Today* **1996**, *16*, 297.

(38) Kunimori, K.; Abe, H.; Yamaguchi, E.; Matsui, S.; Uchijima, T. In *Proceedings of 8th International Congress on Catalysis, V*; 1984; p 251.

(39) Haller, G.; Resasco, D. E. *Adv. Catal.* **1989**, *36*, 173.

(40) Lee, W. H.; Bartholomew, C. H. *J. Catal.* **1989**, *120*, 256.

(41) Jiang, M.; Koizumi, N.; Ozaki, T.; Yamada, M. *Appl. Catal. A* **2001**, *209*, 59.

(42) Toomes, R. L.; King, D. A. *Surf. Sci.* **1996**, *349*, 1.

(43) Mendes, F. M. T.; Perez, C. A. C.; Noronha, F. B.; Schmal, M. *Catal. Today* **2005**, *101*, 45.

(44) Colthup, N. *Introduction to infrared and Raman spectroscopy*, 2nd ed.; Academic Press Inc.: New York, 1975.

(45) Little, L. H. *Infrared Spectra of Adsorbed Species*; Academic Press Inc.: London, 1966.